

Quantum Machine Learning Transition Probabilities in Electronic Excitation Spectra across Chemical Space: The Resolution-vs.-Accuracy Dilemma

Prakriti Kayastha, Sabyasachi Chakraborty, and Raghunathan Ramakrishnan*

Tata Institute of Fundamental Research, Centre for Interdisciplinary Sciences, Hyderabad 500107, India

(Dated: March 31, 2022)

We present a new, high-veracity chemical space dataset—bigQM7 ω —with 12,880 molecules containing up to 7 heavy atoms, and highlight the key challenges in quantum machine learning modeling of electronic excitation spectra. We show excited state modeling with global structural representations to suffer from information overload resulting in diminished structure-property mapping. To improve the signal-to-noise ratio in the modeling, we use locally integrated spectral intensities and highlight a resolution-vs.-accuracy dilemma. Intensities derived from transition probabilities enable quantifying the prediction errors through probabilistic confidence scores. Upon changing the basis set at the target density functional theory level, > 75% confidence score is obtained only at the expense of the resolution, amounting to increasing uncertainties in peak positions. Compared to this, models with state-of-the-art structural representations trained only on < 10% of the data recover the full electronic spectra of the remaining molecules with higher confidence even for sub-nm wavelength resolutions.

I. INTRODUCTION

The future of chemistry research hinges on the progress in data-driven autonomous discoveries[1–3]. The performance of intelligent infrastructures necessary for such endeavors can be tremendously enhanced when augmenting experimental data used for their training with accurate *ab initio* results[4, 5]. For designing opto-electronically important molecules such as dye-sensitized solar cells[6], sunscreens[7, 8], or organic photovoltaics[9, 10], the corresponding target properties are excitation energies and the associated spectral intensities. Accelerated discoveries require a seamless supply of theoretical results to the molecular design workflows. To this end, quantum machine learning (QML) methods have emerged as rapid and accurate surrogates of *ab initio* theories[11–13].

QML collectively stands for data-driven modeling where statistical methods are trained on quantum chemistry big data of molecules/materials. Such models have been shown to accurately forecast a multitude of global[11, 14, 15] and quasi-atomic molecular properties[16–18]. For atomization or bonding energies, their prediction uncertainties are comparable to that of hybrid density functional theory (DFT) approximations[12, 19–24]. QML models of these energies with a robust structural representation benefit from a well-known mapping between the ground state electronic energy and the corresponding minimum energy geometry established by the Hohenberg–Kohn theorem[25]. The Runge–Gross theorem provides a similar mapping between the time-dependent potential and the time-evolved total electron density[26]. However, in QML excited state modeling, the target quantities are state-specific characteristics arising from local

molecular regions. For quasi-atomic properties such as ^{13}C NMR shielding constants[16–18, 27] or K-edge X-ray absorption spectroscopy[16, 27], a representation encoding the local environment of the query atom results in better QML learning rates. For electronic excitations that are also local, the corresponding molecular substructure varies non-trivially across the chemical space. Since QML modeling of electronic excited state properties is performed using global structural representations, such models suffer from an information overload (*i.e.*, poor signal-to-noise ratio) in the feature space amounting to weak structure-property mapping. This effect manifests in unsatisfactory performances of QML models for excitation energies[28, 29], and their zero-order approximations, the frontier molecular orbital (MO) energies[20, 30, 31].

Past studies have focused on excited-state modeling across the chemical space[28, 29, 32] as well as in potential energy surfaces (PESs)[27, 29, 33–35]. A key difference in QML performances in these two application domains is that ambiguities due to atomic indices and size-extensivity that affect the quality of structural representations for chemical space explorations[36, 37] do not arise in PES or dipole surface modeling[38–40], resulting in better learning rates. On a similar note, quasi-particle density-of-states—interpreted as intensities in a photo-emission spectrum—have been successfully modeled[41, 42]. Yet, intensities based on oscillator strengths derived from many-electron excited state wave functions obeying dipole selection rules exhibit slow learning rates[29].

A first step in quantum chemistry big data explorations is selecting a theoretical level accurate for the properties of interest, offering a sustainable high-throughput rate for data generation. For the low-lying excited states of small molecules, equations-of-motion coupled cluster with singles doubles (EOM-CCSD)[43] and approximate second-order coupled-cluster (CC2) deliver a mean error of 0.10–0.15 eV compared to higher-level wave

* ramakrishnan@tifrh.res.in

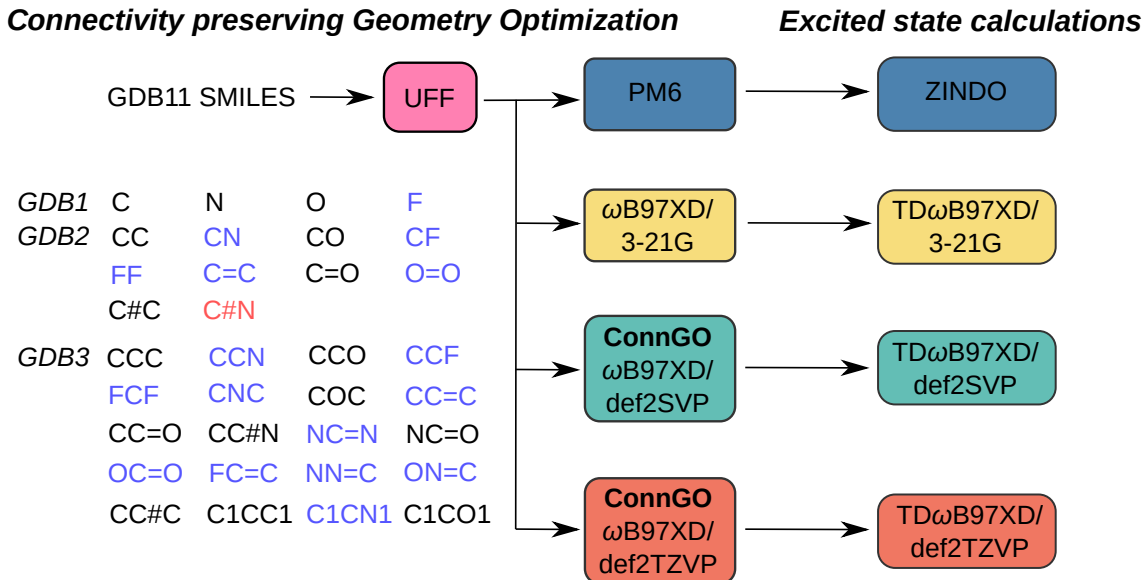


FIG. 1. Chemical space design: Data composition/generation workflows for bigQM7 ω . From the GDB11 dataset, SMILES descriptors for all molecules with up to 7 heavy atoms are collected. For the GDB1-GDB3 subsets, CHONF molecules present in GDB11 but absent in the GDB17 dataset are shown in blue. HCN that is present in GDB17, but absent in GDB11 is shown in red. Initial geometries are obtained with UFF that are subsequently optimized at the PM7 and ω B97XD/3-21G levels. Large basis sets (def2SVP and def2TZVP) ω B97XD geometry optimizations are done using the ConnGO workflow. TDDFT single point calculations are done at the DFT equilibrium geometries, while ZINDO calculations are done at PM6 geometries.

function methods[44–51]. The methods can be made more economical by using the resolution-of-identity (RI) technique, as in RICC2[52] or domain-based local pseudo-natural orbital (DLPNO) variant of EOM-CCSD[53]. These methods, however, have known limitations when modeling the full electronic spectra of thousands of molecules. Formally, the total number of electronic states accounted in these wave function methods scales as $\mathcal{O}(N_o^2 N_v^2)$, where N_o and N_v are the numbers of occupied and virtual MOs. Even for a small molecule such as benzene with a triple-zeta basis set, the size of the resulting electronic Hamiltonian is of the order of millions. Further, the iterative eigensolvers utilized in these calculations converge poorly for higher excited states restricting their usage only to the lowest few excited states[54]. Hence, large scale computations of full electronic spectra across a chemical space dataset are amenable only at the time-dependent(TD) DFT-level[55, 56] that show an $\mathcal{O}(N_o N_v)$ scaling. While DFT offers a suitable high-throughput data generation rate, its accuracy for geometries and properties is dependent on the exchange-correlation (XC) functional. The chemical space dataset, QM9, was designed using the hybrid generalized gradient approximation (hGGA), B3LYP, with the basis set 6-31G(2df,p) because of their use in the G_n family of composite wavefunction methods[57]. For thermochemistry energies, B3LYP that has long served as the chemist’s go-to DFT has an error of 4–5 kcal/mol[58]. A recent benchmark study[59] has shown the range-separated hGGAs (RS-hGGAs) from the ω B97 family[60] to have errors in the 2–3

kcal/mol window; their performance is second only to the G_n methods. Compared to B3LYP, the ω B97 methods also deliver refined molecular structures. While curating the QM9 dataset, the dispersion corrected variant ω B97XD predicted high-veracity geometries less prone to rearrangements in automated high-throughput workflows[61].

In this study, we: (i) Present a high-quality chemical space dataset, bigQM7 ω , containing ground-state properties and electronic spectra modeled at the ω B97XD level with several basis sets. (ii) Introduce transition probabilities that are scaled oscillator strengths for modeling spectral intensities. (iii) Demonstrate the existence of a resolution-vs-accuracy dilemma in continuous spectral modeling. (iv) Evaluate the performance of QML across properties and discuss how excited-states modeling is affected by an information overload in the feature space. (v) Present a QML strategy that enables tuning the information balance with wavelength resolution for accurately reconstructing the full electronic spectra across chemical space.

II. CHEMICAL SPACE DESIGN

A. The bigQM7 ω

Pioneering efforts in small molecular chemical space design produced the graph-based generated dataset, GDB11[62, 63], containing 0.9 billion molecules with up to 11 atoms of CONF. GDB11 provides

TABLE I. Comparison of volume, variety and veracity of selected small molecules chemical space datasets. Size, composition and methods (only DFT or post-DFT) used for data generation are listed.

Details	QM7	QM7b	QM9 ^a	bigQM7 ω
Origin	GDB13	GDB13	GDB17	GDB11
Elements	CHONS	CHONSCl	CHONF	CHONF
Size	7165	7211	133885	12880
Method (Opt.)	PBE0/tight tier-2	PBE/tight tier-2	B3LYP/6-31G(2df,p)	ω B97XD/3-21G ω B97XD/def2SVP ω B97XD/def2TZVP
Method (Freq.)	No	No	B3LYP/6-31G(2df,p)	ω B97XD/3-21G ω B97XD/def2SVP ω B97XD/def2TZVP
Excited states	No	E_1	E_1, E_2, f_1, f_2	all states
Method (Exc.)	No	GW/tight tier-2	RICC2/def2TZVP TDPBE0/def2SVP TDPBE0/def2TZVP TDCAMB3LYP/def2TZVP	TD ω B97XD/3-21G TD ω B97XD/def2SVP TD ω B97XD/def2TZVP

^a Contains 3993/22786 molecules with up to 7/ 8 CONF atoms. Excited state data are available for the 22786 subset Ref.28.

simplified-molecular-input-line-entry-system (SMILES) string-based descriptors encoding molecular graphs. Larger datasets, GDB13[64] and GDB17[65] have since been created containing 13 and 17 heavy atoms, respectively. Synthetic feasibility and drug-likeness criteria eliminated several molecules in GDB13 and GDB17. Starting with the SMILES descriptors presented in GDB13, QM7[11], and QM7b[66] quantum chemistry datasets emerged provisioning computed equilibrium geometries and several molecular properties. Recently, QM7 has been extended by including non-equilibrium geometries for each molecule resulting in QM7-X[67]. The QM9 dataset[68] used SMILES from the GDB17 library reporting structures and properties of 134k molecules with up to 9 atoms of CONF.

In the present work, we explore molecules with up to 7 CONF atoms. We begin with the GDB11 set of SMILES because several important molecules such as ethylene and acetic acid present in GDB11 are filtered out in GDB13 and GDB17. Our new dataset contains 12883 molecules—almost twice as large as the QM7 sets. The breakdown for subsets with 1/2/3/4/5/6/7 heavy atoms is 4/9/20/80/352/1850/10568. The previous datasets QM7, QM7b, and QM9 have been generated using yesteryear’s quantum chemistry workhorses PBE[70], PBE0[44] and B3LYP[71]. Here, we use the RS-hGGA method, ω B97XD[60] that is gaining widespread popularity for its excellent accuracy. Hence, our new dataset is named bigQM7 ω , the last character stands for the DFT approximation utilized. The workflow for high-throughput big data generation is shown in FIG. 1. A summary of properties collected in the form of structured datasets[69] is provided in Table II. A consolidated summary of dataset size, composition, and theoretical levels used for data generation is presented in Table I. As unstructured datasets, we provide raw input/output files[72] to kindle future endeavors.

TABLE II. Structured content of the bigQM7 ω dataset[69]. At various quantum chemistry levels, properties available are listed along with units.

PM6
Equilibrium geometries (Å)
All molecular orbital energies (hartree)
Total electronic and atomization energies (hartree)
ω B97XD/(3-21G, def2SVP, def2TZVP)
Equilibrium geometries (Å)
All molecular orbital energies (hartree)
Atomization energies (hartree)
All harmonic frequencies (cm ⁻¹)
Zero-point vibrational energy (kcal/mol)
Mulliken charges, atomic polar tensor charges (e)
Dipole moment (debye)
Polarizability (bohr ³)
Radial expectation value (bohr ²)
Internal energy at 0 K and 298.15 K (hartree)
Enthalpy at 298.15 K (hartree)
Free energy at 298.15 K (hartree)
Total heat capacity (Cal/mol/K)
ZINDO, TD ω B97XD/(3-21G, def2SVP, def2TZVP)
Excitation energy of all states (eV, nm)
Oscillator strengths of all excitations (dimensionless)
Transition dipole moment of all excitations (au)

B. Computational Details

Initial structures for the 12883 molecules in bigQM7 ω were generated from SMILES by relaxing with the universal force field (UFF)[73] employing tight convergence criteria using OpenBabel[74]. As a guideline for quantum chemistry big data generation, a previous study proposed connectivity preserving geometry optimizations (ConnGO) to eliminate structural ambiguities due to rearrangements encountered

in automated high-throughput calculations[61]. Accordingly, we used a 3-tier ConnGO workflow to generate geometries at the ω B97XD DFT level using def2SVP and def2TZVP basis sets. Geometry optimizations at the simpler levels PM6 and ω B97XD/3-21G were performed without ConnGO starting with the UFF structures. For ω B97XD/def2SVP final geometries, we used HF/STO3G and ω B97XD/3-21G as intermediate tier-1 and tier-2 levels, respectively. Similarly, for ω B97XD/def2TZVP, HF/STO3G and ω B97XD/def2SVP were lower tiers. In each tier, ConnGO compares the optimized geometry with the covalent bonding connectivities encoded in the initial SMILES and detects molecules undergoing rearrangements. For this purpose, we used the ConnGO thresholds 0.2 Å for the maximum absolute deviation in covalent bond length and a mean percentage absolute deviation of 6%. At both ω B97XD/def2SVP and ω B97XD/def2TZVP levels, 3 molecules with the SMILES `O=c1cconn1`, `N=c1nconn1`, `O=c1nconn1`, failed the ConnGO connectivity tests. Further investigation revealed these molecules to contain an -NNO- substructure in a 6-membered ring facilitating dissociation as previously seen in Ref.61. After removing these molecules, the size of bigQM7 ω stands at 12880.

Using geometries at four levels of theory, we performed vertical excited-state calculations at the Zerner’s intermediate neglect of differential overlap (ZINDO) and TD ω B97XD levels. ZINDO calculations were done on PM6 minimum energy geometries, while TD ω B97XD with 3-21G, def2SVP, and def2TZVP basis sets, at the corresponding ground state equilibrium geometries. All electronic structure calculations were performed using the Gaussian suite of programs[75]. In DFT calculations, `tight` optimization thresholds and `ultrafine` grids were used for evaluating the exchange-correlation (XC) energy. Very few molecules required relaxing the optimization thresholds for monotonic convergence towards a minimum. All final geometries were confirmed to be local minima through harmonic frequency analysis. For highly symmetric and molecules with multiple triple bonds, converging to minima was only possible with the `verytight` optimization threshold and `superfine` grids.

III. METHODS

A. Kernel Ridge Regression: Standardized Scores for Multi-Property Learning

Kernel ridge regression (KRR) based QML (KRR-QML) enables accurate predictions through an exact global optimization of a convex statistical model[11, 12, 76]. In KRR-QML the target property, t_q , of an out-of-sample query, q , is estimated as the linear combination of kernel (or radial basis) functions, each centered on a training entry. Formally, with a suitable choice of the kernel function, KRR approaches the target

when the training set is sufficiently large

$$t_q = \lim_{N \rightarrow \infty} \sum_{i=1}^N c_i k(\mathbf{d}_q - \mathbf{d}_i). \quad (1)$$

The coefficients, $\{c_i\}$, are obtained by regression over the training data. The kernel function, $k(\cdot)$, captures the similarity in the representations of the query, q , and all N training examples. For ground state energetics, the Faber-Christensen-Huang-Lilienfeld (FCHL) formalism in combination with KRR-QML has been shown to perform better than other structure-based representations[20, 77]. However, for excitation energies and frontier MO gaps, FCHL’s performance drops compared to the spectral London-Axilrod-Teller-Muto (SLATM) representation[78]. In this study, we compare and contrast the performance of FCHL and SLATM for various electronic properties. SLATM delivers best accuracies with the Laplacian kernel, $k(\mathbf{d}_q, \mathbf{d}_i) = \exp(-|\mathbf{d}_q - \mathbf{d}_i|_1/\sigma)$, where σ defines the length scale of the kernel function and $|\cdot|_1$ denotes L_1 norm. For the FCHL formalism, we found an optimal kernel width of $\sigma = 5$ through scanning and a cutoff distance of 20 Å was used to capture the global structure of heptane, the longest molecule in bigQM7 ω .

The kernel width, σ , is traditionally determined through cross-validation. For multi-property modeling σ can be estimated using the ‘single-kernel’ approach[14], where σ is estimated as a function of the largest descriptor difference in a sample of the training set, $\sigma = \max\{d_{ij}\}/\log(2)$. Previous works[14, 18, 79] have shown single-kernel modeling to agree with cross-validated results with in the uncertainty arising due to training set shuffles. KRR with a single-kernel facilitates seamless modeling of multiple molecular properties using standard linear solvers

$$[\mathbf{K} + \zeta \mathbf{I}][\mathbf{c}_1, \mathbf{c}_2, \dots] = [\mathbf{p}_1, \mathbf{p}_2, \dots], \quad (2)$$

where \mathbf{p}_j is j -th property vector and \mathbf{c}_j is the corresponding regression coefficient vector. We use Cholesky decomposition that offers the best scaling of $2N^3/6$ for dense kernel matrices of size N [80]. The diagonal elements of the kernel matrix are shifted by a positive hyperparameter, ζ to regularize the fit, *i.e.*, prevent over-fitting. We note in passing that conventionally the regularization strength is denoted by the symbol λ , which we reserve in this study for wavelength. Another role of ζ is to make the kernel matrix positive definite if there is linear dependency in the feature space arising either due to redundant training entries or due to poor choice of representations. Even in the absence of linear dependency, it is useful to condition the kernel matrix, hence we set ζ to 10^{-4} . We generated SLATM representation vectors and the FCHL kernel using the QML code[81], and performed all other QML calculations using in-house programs written in Fortran. All QML errors reported in this study are based on 20

shuffles of the data to prevent selection bias for small training set sizes.

In Section IV C, we compare the KRR-QML errors for selected ground and excited-state properties with different physical units and magnitudes. To compare the offsets in a learning curve and rate of learning across molecular properties, one can use mean percentage errors[79, 82], or by scaling by the maximal value[14]. Both strategies have drawbacks: percentages are not defined when the property values are zero or near-zero, while the maximal value is affected by outliers. Hence, in this study, we transform properties to their standard scores, $-1 \leq z \leq +1$ as done in data science[83]. The standard score accounts for the sample mean, μ_j and standard deviation, s_j , given as

$$\mathbf{z}_j = \frac{\mathbf{P}_j - \mu_j}{s_j}. \quad (3)$$

Out-of-sample QML errors calculated in units of s_j enable meaningful comparisons of error rates across various properties.

B. Electronic Transition Probabilities

For practical applications of QML to electronic spectra it is pertinent that the intensities are also quantitatively predicted alongside energies/wavelengths. Conventionally, the band intensity due to the k -th excitation is the molar absorption coefficient that is proportional to the corresponding oscillator strength, $f_{0 \rightarrow k}$, denoted shortly as f_k [84]. For full spectrum modeling, each value of f_k is a separate target quantity. Errors for multiple f_k can be meaningfully compared using standard scores. However, it is advantageous to directly model on the normalized oscillator strengths that also result in the same standard scores defined as

$$p_k = \frac{f_k}{\sum_k f_k}. \quad (4)$$

This new target quantity, p_k corresponds to the transition probability of k -th excitation offering a total probabilistic error metric, bound in $[0, 1]$, for predicting the full spectrum.

For organic molecules such as those in bigQM7 ω , a complete electronic spectrum spans the wavelength range of $\lambda \leq 850$ nm. The average number of states in a spectrum at the ω B97XD/def2TZVP target level is as large as 3.5k facilitating p_k to be treated as a continuous distribution $p(\lambda)$. In the full wavelength range of a spectrum, $\lambda_{\text{spectrum}}$, the quantity, $p(\lambda)d\lambda$, signifies the probability of an excitation in an infinitesimal wavelength range. When integrating $p(\lambda)$ over $\lambda_{\text{spectrum}}$, the probability of excitation is 1.0 for all molecules.

In practice, one is interested in transition probabilities at smaller resolutions, $\Delta\lambda$. We uniformly divide the spectral range in powers of 2, $\Delta\lambda = \lambda_{\text{spectrum}}/N_{\text{bin}}$,

where $N_{\text{bin}} = 1, 2, 4, \dots$ is the number of bins. Our target is the sum of transition probabilities, P , in a bin

$$P(\lambda_a) = \sum_{k=1}^{\text{all states}} p_k(\lambda_k), \quad (5)$$

where $\lambda - \Delta\lambda/2 < \lambda_k \leq \lambda + \Delta\lambda/2$, a is the bin index, and λ_a is the central wavelength of the bin. To compare a predicted full spectra with a reference, we introduce the total mean absolute error (MAE) per molecule summed over all bins:

$$\text{MAE}(\Delta\lambda) = \frac{1}{N_{\text{mol}}} \sum_{i=1}^{N_{\text{mol}}} \sum_{a=1}^{N_{\text{bin}}} |P^{\text{ref.}}(\lambda_a) - P^{\text{pred.}}(\lambda_a)|. \quad (6)$$

The upper bound of the absolute deviation, $|P^{\text{ref.}}(\lambda_a) - P^{\text{pred.}}(\lambda_a)|$, is set to 1 for conservation of probability. Final performances are evaluated using a total confidence score, Φ , for the full spectrum at a given resolution, $\Delta\lambda$

$$\Phi(\Delta\lambda) = 100 \times [1 - \text{MAE}(\Delta\lambda)], \quad (7)$$

the factor 100 makes the score in %. The error is exactly zero when $\Delta\lambda = \lambda_{\text{spectrum}}$ resulting in the maximum confidence score, $\Phi(\lambda_{\text{spectrum}}) = 100\%$.

In Section IV B, for the full spectra of all molecules in bigQM7 ω , $P(\lambda_a)$ calculated at the ω B97XD/def2TZVP level are used as the target, and confidence scores of other methods are evaluated at various wavelength resolutions. Similarly, in Section IV D, for the same target we report out-of-sample confidence scores of SLATM and FCHL predictions of full electronic spectra for various training set sizes.

IV. RESULTS AND DISCUSSIONS

A. Quantum Chemistry Benchmarks for Excited State Properties

The ‘mountaineering efforts’ have reported extended excited states benchmarks of highly accurate wavefunction methods for carefully selected sets of few hundred molecules[48, 49, 51]. However, for excited state modeling of the bigQM7 ω dataset, these highly accurate methods are prohibitively expensive. Hence we resort to TDDFT methods for modeling the complete electronic excitation spectra. To choose an accurate XC functional, we select the smallest 33 molecules with up to 3 heavy atoms as a benchmark set. We compare the accuracies of thirteen XC functionals—SVWN5[85], PW91[86], BLYP[87], TPSS[88], B3LYP[71], PBE0[44], TPSSH[88], M062X[89], M11[90], LC-BLYP[91], LC- ω HPBE[92], CAM-B3LYP[93], and ω B97XD[60]—from several levels of the Jacob’s ladder[94].

Using the accurate canonical STEOM-CCSD method as the reference, we find ω B97XD to deliver the smallest

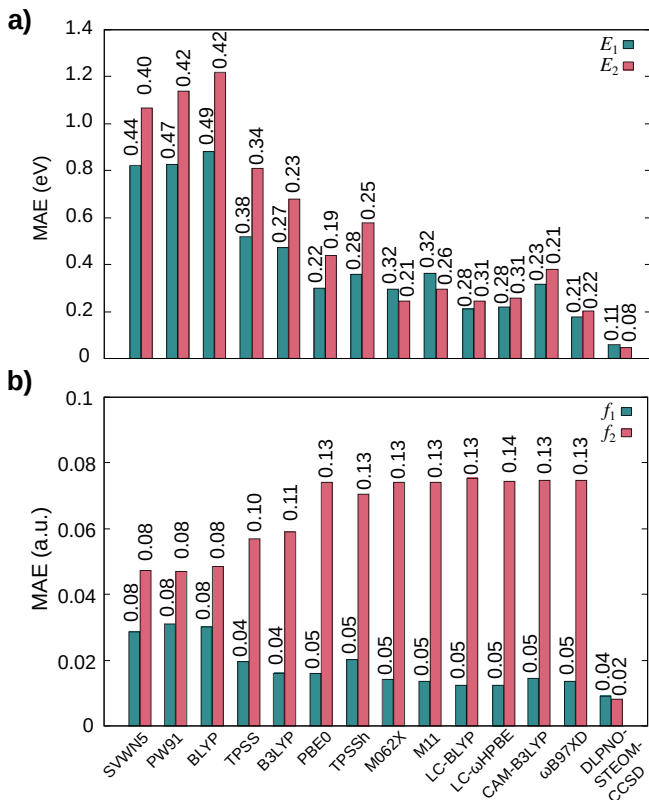


FIG. 2. Error metrics for selected methods for the lowest two excitations compared to STEOM-CCSD. Results are presented for 33 entries in bigQM7 ω with up to three CONF atoms. All results are for the def2TZVP basis set. Mean absolute errors (MAEs) are reported for a) excitation energies (E_1 , E_2), and b) oscillator strengths (f_1 , f_2). Root mean square deviations are provided above the histograms. Singlet O₂ was excluded for SVWN5, BLYP and TPSS because of density convergence failure.

MAE of 0.18 ± 0.21 and 0.20 ± 0.22 eV, for E_1 and E_2 , respectively, see FIG. 2a. The long-range corrected GGA (LC-GGA), LC-BLYP gives lower MAEs (0.21 ± 0.28 and 0.25 ± 0.31 eV) compared to the LC-hGGA method CAM-B3LYP (0.32 ± 0.23 and 0.38 ± 0.21 eV). This is because the MAE of the latter method is influenced by systematic errors. The standard deviation of CAM-B3LYP, however, is smaller than that of LC-BLYP. We also find the DLPNO-STEOM-CCSD method to have errors of 0.06 ± 0.11 and 0.049 ± 0.081 eV. Approximating STEOM-CCSD with DLPNO results in very small errors of 0.05 ± 0.04 , and 0.08 ± 0.02 for f_1 and f_2 , respectively. Since oscillator strengths are non-variational, across methods the character of the chromophore participating in the excitation can swap. This artifact influences the character of f_2 going from STEOM-CCSD to TDDFT methods resulting in larger errors (see FIG. 2b). In this work, we use ω B97XD as the preferred choice for excited state calculations.

The quantity, $\sum_k f_k$, is a global property suitable for data-driven modeling with global representations. For

an exact excited state method this sum according to the Thomas–Reiche–Kuhn (TRK) theorem must converge to the number of electrons[84]. In quantum chemistry, unfortunately, this condition is satisfied only at the full-CI limit, when all excitations (singles, doubles, triples, and so on) are accounted for at the basis set limit. Hence, ZINDO and the TD ω B97XD used here are not expected to satisfy the TRK limit. We illustrate this aspect in FIG. 3 where the TRK-sum, $\sum_k f_k$, is plotted as a function of number of allowed states at the ZINDO and TDDFT levels. ZINDO deviates the most from the target TD ω B97XD/def2TZVP because the number of excited states available is limited by two factors. Firstly, in the ZINDO model core electrons are not included. Secondly, semi-empirical models are implicitly based on a minimal basis set.

TDDFT modeling with 3-21G improves the magnitude of $\sum_k f_k$ as well as the total number of states. With the def2SVP and def2TZVP basis sets, $\sum_k f_k$ appears to quantize at even numbers with a separation of about 2. For the large basis set, def2TZVP, the number of accessible states increases as expected, while the TRK-sum drops below the def2SVP values. We investigated the reason for this trend using methane as a test case and found the def2- basis sets to show oscillatory convergence with the basis set size. For methane, the

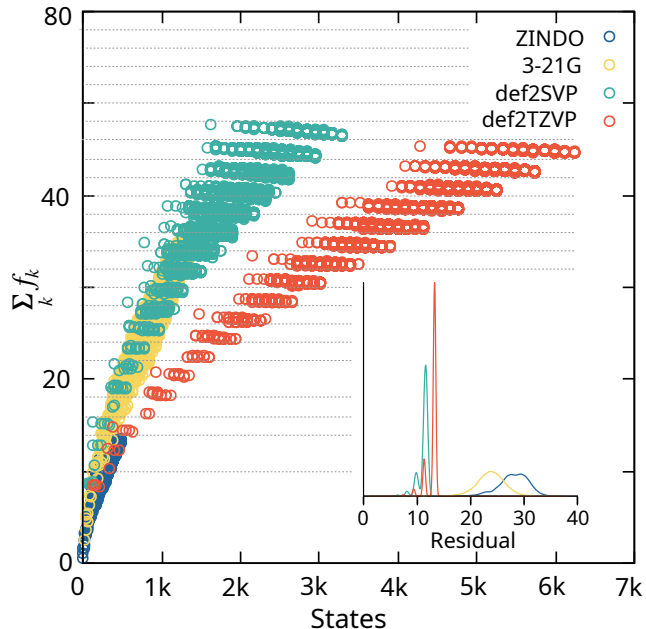


FIG. 3. Basis set effect on oscillator strength sums for bigQM7 ω molecules at TD ω B97XD. Sum of oscillator strengths is plotted against number of allowed excitations from the ground electronic state with 3-21G, def2SVP and def2TZVP basis sets. ZINDO values are also shown for comparison. Horizontal lines mark the Thomas-Reiche-Kuhn limit an exact excited state method must coincide with. The inset shows the distribution of deviation of oscillator strength sums from number of electrons, N_e .

def2SVP/def2TZVP values are 8.78/8.26, the larger basis set value agreeing better with the aug-cc-pV5Z basis set limit value at 7.82. At def2TZVP, the degree of quantization improves with points better approaching integer values. Residual errors in ZINDO/TDDFT TRK-sums from N_e are shown in the inset to FIG. 3.

B. Resolution-vs.-Accuracy Trade-off

Typically, uncertainties of hybrid-DFT approximations compared to higher-level wavefunction methods are used as threshold accuracies for QML modeling. For total energies and excitation energies, these values are 3 – 4 kcal/mol[59], and 0.2 – 0.3 eV[51], respectively. For oscillator strengths, such a threshold is not established, especially for chemical space datasets. For the bigQM7 ω dataset, we establish a desired target accuracy for modeling full spectral transition probabilities using confidence scores for ZINDO, ω B97XD/3-21G, or ω B97XD/def2SVP compared to ω B97XD/def2TZVP, see FIG. 4. The electronic spectra of molecules in bigQM7 ω span a wavelength range until 850 nm with > 99% of the oscillator strength values falling in the deep UV to X-ray range ($\lambda \leq 120$ nm). Such a trend has been noted before for small organic molecules[95]. Hence in this study, we fix the spectral range ($\lambda_{\text{spectrum}}$) to 0–120 nm and determine transition probabilities according to Eqs. 4 and 5. For a given wavelength resolution, transition probabilities are compared across methods and confidence scores are calculated according to Eq. 7. For a meaningful comparison of results across basis sets, we also account for systematic shifts. For the limiting case of $\Delta\lambda = 120$ nm, ZINDO, ω B97XD/3-21G, and ω B97XD/def2SVP methods approximate the target ω B97XD/def2TZVP values with a confidence score of 100% because the total probability is 1 at all levels. The number of bins, N_{bin} , is increased in powers of 2 until sub-nm resolutions are reached.

With increasing resolution, the methods diverge from the target, ZINDO showing the largest deviation. Both small basis set TDDFT results to follow very similar trends until ≈ 1 nm. For a resolution of 1% of $\lambda_{\text{spectrum}}$, $\Delta\lambda = 1.2$ nm, 3-21G/def2SVP predictions have a confidence of 50 – 60% compared to the target, while ZINDO has a worse score $\approx 30\%$. For $\Delta\lambda = 0.94$ nm the agreement between the TDDFT results is with a confidence score of 40 – 50%. For a semi-quantitative confidence score of 75% with the target, ZINDO requires a resolution of 20 nm. At the ω B97XD TDDFT-level, when decreasing the quality of the basis set from def2TZVP to 3-21G or def2SVP 75% confidence scores are obtained only for resolution of 6–7 nm indicating the resolution-vs.-accuracy trade-off.

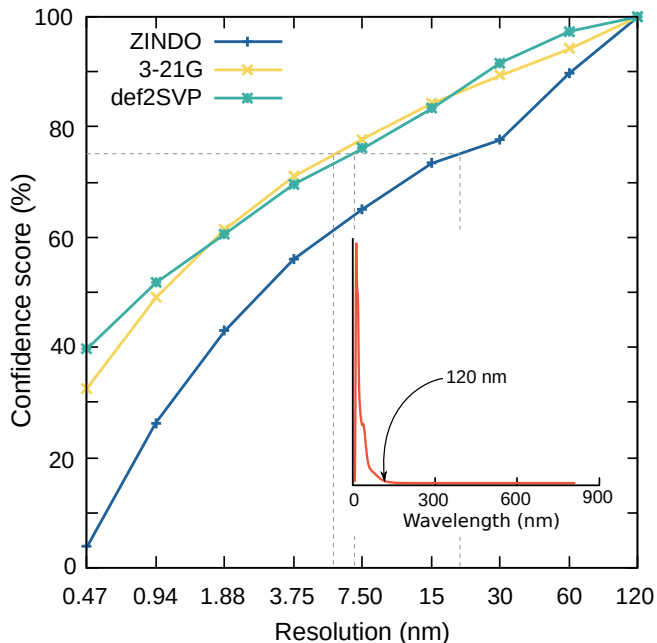


FIG. 4. Confidence scores (see Eq. 7) for transition probabilities in the $\lambda \leq 120$ nm range for all molecules in bigQM7 ω . The scores are shown for ZINDO, ω B97XD/3-21G and ω B97XD/def2SVP levels for varying wavelength resolution ($\Delta\lambda$) for approximating the ω B97XD/def2TZVP level values. Inset shows the distribution of reference ω B97XD/def2TZVP values.

C. Critical Analysis of QML for Ground and Excited State Properties

We compare the learning rates of atomization energy (E), lowest excitation energy (E_1), its corresponding oscillator strength (f_1), and the TRK-sum ($\sum_k f_k$) at the ω B97XD/def2TZVP level for the bigQM7 ω dataset. For all four properties at the ω B97XD/def2TZVP level in Fig. 5, the error rates are reported for the standard scores (\mathbf{z}_j) of the corresponding properties (\mathbf{p}_j) defined in Eq.3. Learning rates based on \mathbf{z}_j enable interpretation of out-of-sample errors in units of the standard deviation of the corresponding target. Hence, the offset at the zero training set size limit, $N = 0$, of a learning curve based on MAE must coincide with the standard deviation of \mathbf{z}_j . The advantage is that across multiple properties, the learning rates are made comparable.

The performance of QML models depends on the extent of mapping between the target property and the representation. E has the well-established mapping to the total ground state electron density that is mapped to the global molecular structure. Only a fraction of the total electron density is perturbed during excitations. Hence, a representation for modeling E_1 must only encode the corresponding change in the electron density distribution and the associated local molecular structure. While it is possible to characterize valence excited-states for molecules with known functional groups[96], it is

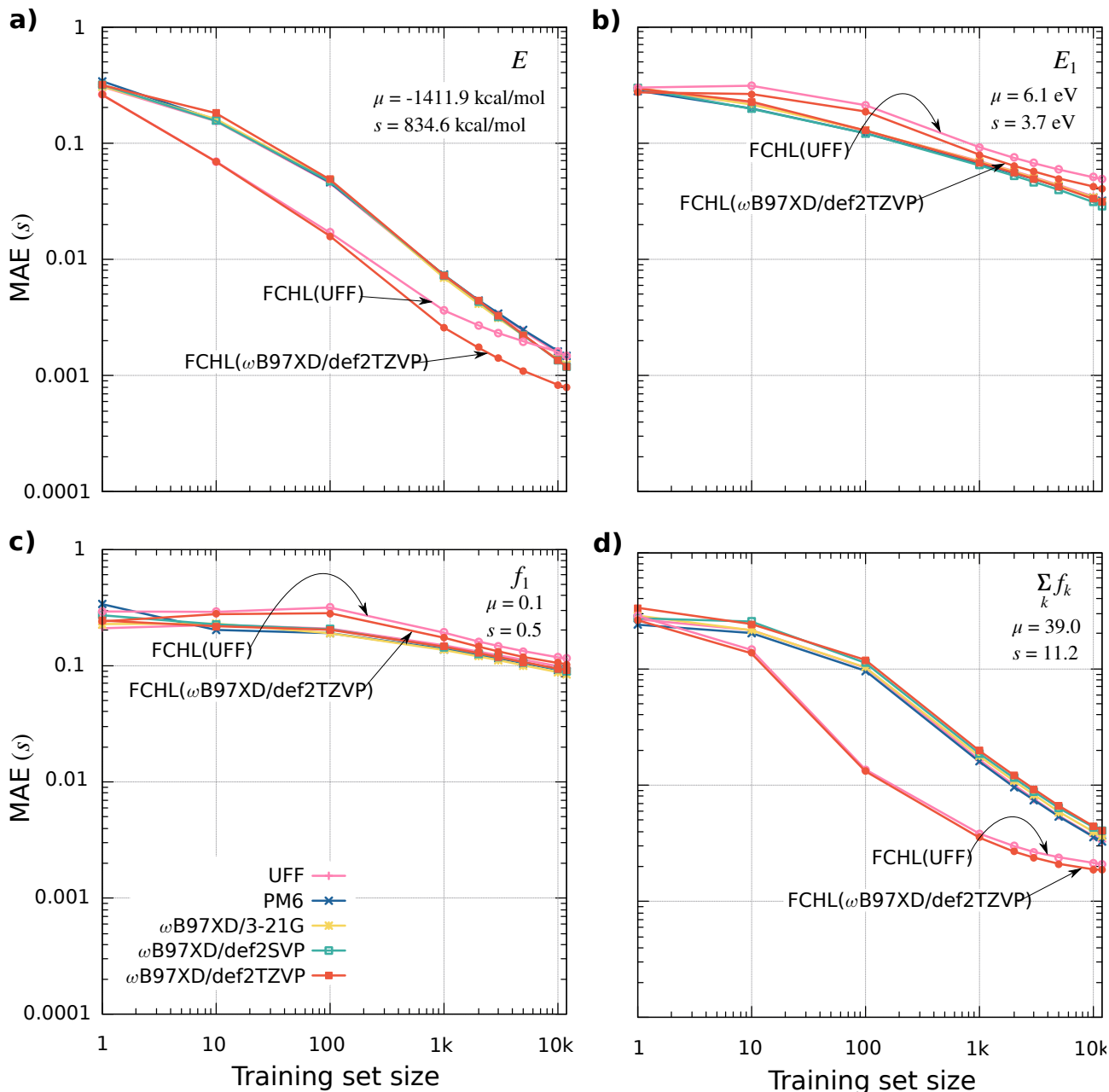


FIG. 5. Multi-property learning curves for the bigQM7 ω dataset using descriptors made with geometries at different levels. For each property, SLATM-QML models are made using geometries at 5 levels defined in panel c). Out-of-sample mean absolute errors (MAEs) are shown with varying training set size: a) DFT atomization energy (E), b) TDDFT lowest excitation energy (E_1), c) TDDFT oscillator strength of the lowest excitation (f_1), and d) sum of f_k over all states. In all cases, target properties are at the ω B97XD/def2TZVP level. MAE per property is calculated using the standard score defined in Eq. 3. Sample mean (μ) and sample standard deviation (s) are calculated using random 1k entries. For comparison, QML results based on the FCHL descriptor are also provided.

hard to automate this task for high-throughput chemical space design. Hence, predominant of the global structure provided to QML has no relevance for modeling excited state properties. This additional information has to be considered as a noise in the representation.

For QML modeling of E , FCHL was found to deliver the least error among several representations while for

orbital energies SLATM was found to perform better[20]. The target property E is dependent on the global molecular structure resulting in better predictions, hence both representations yield good accuracies, see FIG. 5a. However, for E_1 , the global structural descriptors contain extraneous information not relevant for the target. Due to this diminished signal-to-noise ratio, QML models

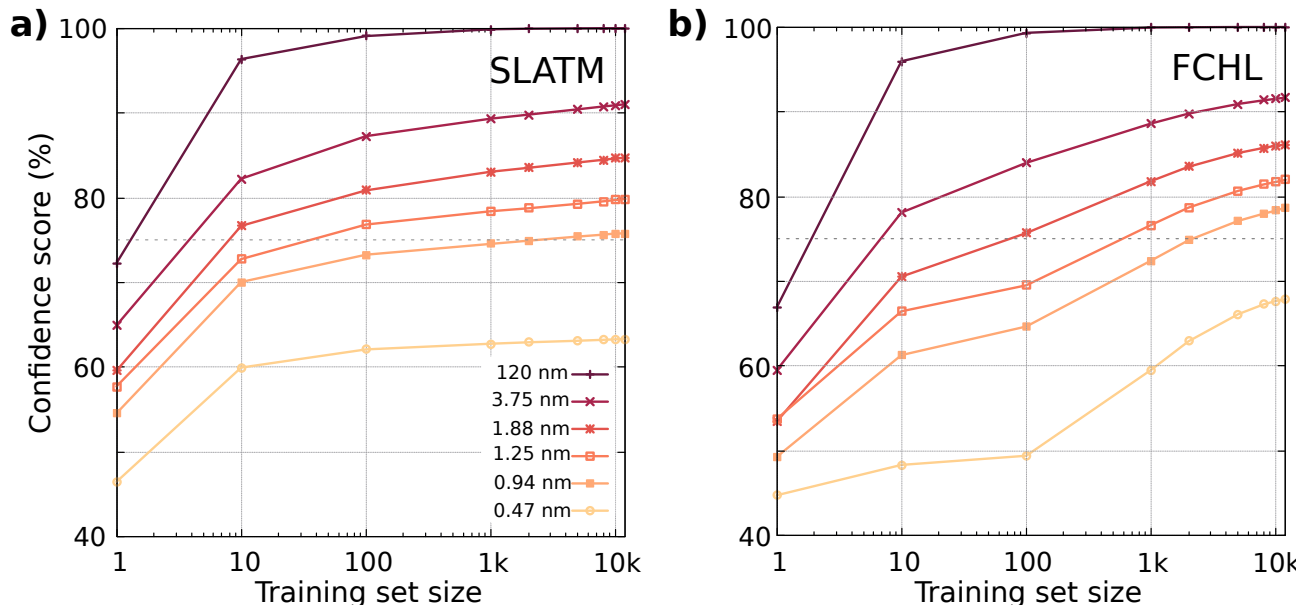


FIG. 6. Out-of-sample confidence scores for predicting ω B97XD/def2TZVP level transition probabilities (in the ≤ 120 nm region) for the bigQM7 ω dataset. QML models were trained using the single-kernel approach with the SLATM (a) and FCHL (b) representations generated using UFF-level geometries. For each curve, the QML target is a vector of length N_{bin} , modeled simultaneously with single-kernel. Horizontal dashed line meets the learning curve for a score of 75%.

yield relatively poor accuracies for E_1 compared to E , see FIG. 5b. It is interesting to note that while FCHL delivers better accuracies for E compared to SLATM, the trend is reversed for E_1 .

When the structure-to-property mapping is weak, the error in FCHL modeling is amplified—implying the model to be ‘stiff’. In numerical applications, stiff models are common. For example in micro-kinetic modeling of reaction rates, the corresponding equations are stiff differential equations[97]. The output of stiff models are more sensitive to small changes in the input, making them mathematically ill-conditioned[98]. For FCHL modeling of target TD ω B97XD/def2TZVP level properties, geometries at the same level delivers lower errors compared to geometries from UFF. This trend also reflects on the stiff nature of FCHL. On the other hand, SLATM is insensitive to the subtle differences between geometries across methods resulting in similar learning rates for geometries relaxed at UFF, PM6, or DFT levels, see Figs. 5a and 5b. The performance of FCHL and SLATM models are poor for f_1 , FIG. 5c. This is because all details of the global structure encoded in the geometry is not relevant for the target property as in the case of E_1 . Such poor learning rates for f_1 was noted in QML modeling of ‘brown carbon’ molecules that are atmospheric pollutants as in aerosols[29]. As in the case of E_1 , FCHL’s performance for f_1 is inferior compared to that of SLATM. UFF geometry performs worse than the target-level geometries when using FCHL.

The fourth property modeled is the TRK-sum, $\sum_k f_k$. Individual oscillator strengths arise from different local regions of a molecule. When summed, the property is

global, resulting in lower QML errors than for both E_1 and f_1 (FIG. 5d). Since the TRK-sum has a better mapping to the global geometry, as in the case of E , the performance of the FCHL representation outperforms SLATM.

For the smallest model with $N = 1$, the errors for both representations and all four properties are in the 0.2 – 0.3 range. With SLATM, the learning curves for E converge to 0.001 – 0.002 units of the property standard deviation, s . For the largest model with 12k training examples, this error amounts to 8 kcal/mol for the remaining 880 out-of-sample molecules. With UFF geometries, FCHL’s errors are similar to that of SLATM. With FCHL, the error drops to 0.0008 $s = 5$ kcal/mol when using target level geometries. For both E_1 and f_1 , we find better learning rates with SLATM compared to FCHL. The learning rate for E_1 is inferior to E reaching 0.03 s with SLATM. Compared to this, the error rates for f_1 are about three-fold larger reaching 0.1 s at the 12k limit. For TRK-sum, the qualitative trends in QML performance is comparable to that of E . Target-level geometries deliver the best performance with FCHL reaching 0.002 s at the 12k limit. Changing the geometry to the UFF level only incurs a small increase in the error while the cost of FCHL kernel generation is three orders of magnitude smaller. The rest of this study focuses on transition probabilities that are normalized oscillator strengths for which we perform QML modeling using SLATM and FCHL representations with geometries from the inexpensive UFF level.

D. QML Modeling of Transition Probabilities and Reconstruction of Electronic Spectra

In FIG. 6, we present benchmark learning rates for QML modeling on transition probabilities in the $\lambda \leq 120$ nm wavelength range at various resolutions with SLATM and FCHL representations. For models with $N < 1k$, SLATM delivers higher confidence scores compared to FCHL. The performance of both these models are similar for $N \approx 1k$. Beyond 1k, SLATM’s predictions saturate faster than FCHL. For the semi-quantitative resolution, $\Delta\lambda = 1.88$ nm, SLATM predictions reaches a confidence of 80% at $N < 100$ while FCHL reaches this score at $N = 400$. However, at the $N = 12k$ limit, FCHL’s score exceeds that of SLATM. For a higher resolution with $\Delta\lambda = 1.25$ nm, a score of 80% is reached at $N = 12k$ and $N = 4k$ with SLATM and FCHL, respectively. For the sub-nm resolution, $\Delta\lambda = 0.94$ nm, SLATM and FCHL models with 1k training examples (less than 10% of the dataset) reach a score of 74% and 71%, respectively. For transition probabilities our findings suggest the suitable resolution to be 0.94 nm, less than 1% of the spectral range of 120 nm. At this resolution, transition probabilities from the TD ω B97XD/def2SVP level agrees with the target-level only with a score of about 50% (see FIG. 3). The confidence score drops even further for TD ω B97XD/3-21G and ZINDO levels. Further increase in the resolution to 0.47 nm results in worse predictions highlighting the resolution-vs-accuracy dilemma in QML full spectrum modeling. Hence, Δ -QML models[15] based on these baselines are expected to perform inferiorly than a direct model trained on the target-level spectra. We confirmed this through separate QML calculations.

Using a 1k FCHL model based on UFF geometries, we reconstruct the full electronic spectrum at the sub-nm resolution $\Delta\lambda = 0.94$ nm for four random out-of-sample molecules, see FIG. 7. In order to compare the individual spectra with the absolute heights from experimental intensities, one can scale the predicted transition probabilities by the TRK-sum of each molecule that can be separately predicted by another QML model. For an exact *ab initio* method, the TRK-sum should be N_e . However, the TDDFT-level TRK-sum underestimates this limit due to the absence of double and higher excitations. Hence, to empirically reach the experimental intensities, here we scale the QML predicted transition probabilities by N_e .

The reconstructed spectra of all four molecules agree well with the reference in the core region ($\lambda < 25$ nm). The spectral reconstruction in the $\lambda = 25 - 120$ nm wavelength range is relatively poor because of decreasing electronic density of states. The valence spectra, $\lambda > 120$ nm, of the bigQM7 ω molecules is further under-represented. At 1k, the confidence score of FCHL for 12k out-of-sample molecules is 72% for $\Delta\lambda = 0.94$ nm (see FIG. 6b). Compared to this performance, three molecules presented in FIG. 7 show better scores.

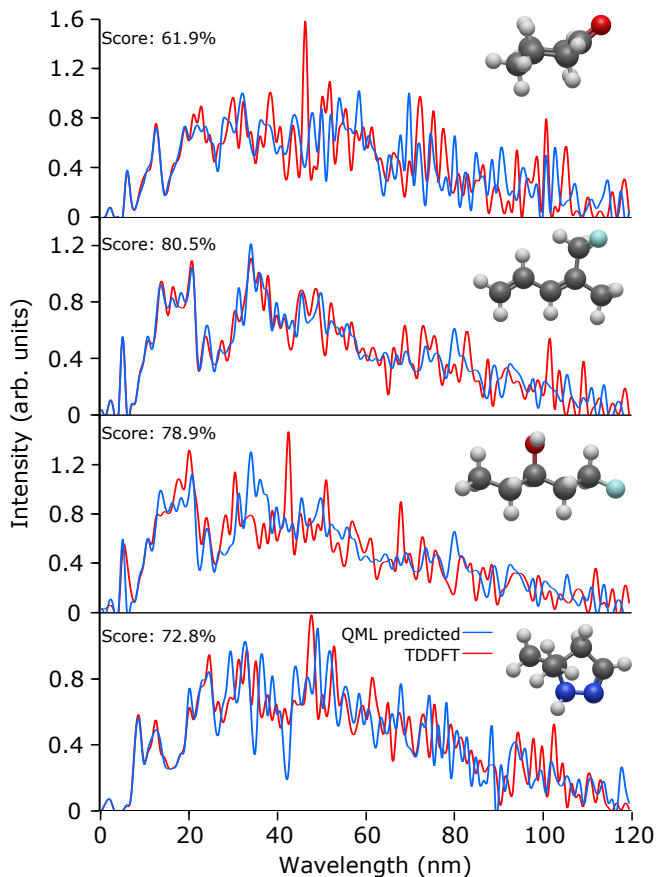


FIG. 7. Electronic excitation spectrum of four randomly selected molecules—cyclohexanone, (3Z)-5-fluoro-4-methylpenta-1,3-diene, 1-fluoropentan-3-ol, and 5,5-dimethyl-4,5-dihydro-1H-pyrazole—reconstructed at 0.94 nm resolution using a 1k FCHL-KRR-ML. Training was done with the TD ω B97XD/def2TZVP target-level transition probabilities in the wavelength range ($\lambda \leq 120$ nm). Confidence scores compared to DFT reference values are also given. For clarity, both DFT and QML predicted spectra are presented as cubic spline interpolations.

The confidence score for cyclohexanone is less than the model’s mean performance. The score improves to 66% when the training set is increased to 2k. Based on the benchmarks discussed above, one can expect improved predictions at larger training sets and with target-level geometries with the FCHL kernel albeit at a higher cost.

V. CONCLUSIONS

In this work we present the new chemical space dataset, bigQM7 ω , containing 12880 molecules with up to 7 atoms of CONF. Geometry optimizations of the bigQM7 ω molecules have been performed with the ConnGO workflow ensuring veracity in the covalent bonding connectivities. Minimum energy geometries, harmonic vibrational wavenumbers, and excited state calculations are reported with the accurate,

range-separated hybrid DFT method ω B97XD, and the def2TZVP basis set. For all molecules, full electronic spectra are calculated covering all possible excitations allowed by the TDDFT framework. For the low-lying excited states of the bigQM7 ω molecules, we have benchmarked various DFT methods against the highly accurate STEOM-CCSD level and found ω B97XD/def2TZVP to be best choice. We discuss the well-known limitation of TDDFT approximations for satisfying the Thomas–Reiche–Kuhn sum rule and illustrate the residual error in various methods.

We shed new light on the performance of popular representations SLATM and FCHL for modeling the valence excitation energies and oscillator strengths. Our results suggest the FCHL model to be stiffer compared to SLATM delivering accurate predictions only for properties that map to the global molecular structure. For excited state properties arising from local molecular regions, we report better accuracies with SLATM. For QML modeling of the full electronic spectra, we propose an approach using transition probabilities locally integrated at various wavelength resolutions. We illustrate the existence of a resolution-vs.-accuracy dilemma for comparing full electronic spectra from different methods. Semi-quantitative agreement between methods is reached only at the expense of resolution. Compared to this, QML models deliver better accuracies at a sub-nm resolution when training on fraction of the dataset. For accurate reconstruction of full electronic spectra across chemical space with a resolution of < 1 nm, we recommend FCHL-KRR-QML trained on

transition probabilities. Further, it may be possible to improve the QML model’s performance in the long wavelength region using varying resolutions at different spectral regions.

Improvements of QML modeling of excited state requires development of new local descriptors. For this, an automated protocol to characterize electronic excited-states should be developed for high-throughput chemical space design frameworks. All structured and unstructured data provided along with this study should aid future data-driven efforts.

VI. DATA AVAILABILITY

Structures, ground state properties and electronic spectra of the bigQM7 ω dataset are available at <https://moldis-group.github.io/bigQM7w>, see Ref.69. Input and output files of corresponding calculations are deposited in the NOMAD repository (<https://dx.doi.org/10.17172/NOMAD/2021.09.30-1>), see Ref.72.

VII. ACKNOWLEDGMENTS

We acknowledge support of the Department of Atomic Energy, Government of India, under Project Identification No. RTI 4007. All calculations have been performed using the Helios computer cluster, which is an integral part of the MolDis Big Data facility, TIFR Hyderabad (<http://moldis.tifrh.res.in>).

-
- [1] S. Steiner, J. Wolf, S. Glatzel, A. Andreou, J. M. Granda, G. Keenan, T. Hinkley, G. Aragon-Camarasa, P. J. Kitson, D. Angelone, *et al.*, *Science* **363** (2019).
- [2] M. Christensen, L. P. Yunker, F. Adedjeji, F. Häse, L. M. Roch, T. Gensch, G. dos Passos Gomes, T. Zepel, M. S. Sigman, A. Aspuru-Guzik, *et al.*, *Commun. Chem.* **4**, 1 (2021).
- [3] E. Stach, B. DeCost, A. G. Kusne, J. Hattrick-Simpers, K. A. Brown, K. G. Reyes, J. Schrier, S. Billinge, T. Buonassisi, I. Foster, *et al.*, *Matter* (2021).
- [4] X. Li, P. M. Maffettone, Y. Che, T. Liu, L. Chen, and A. Cooper, *Chem. Sci.* (2021).
- [5] Y. Bai, L. Wilbraham, B. J. Slater, M. A. Zwijnenburg, R. S. Sprick, and A. I. Cooper, *J. Am. Chem. Soc.* **141**, 9063 (2019).
- [6] S. Mathew, A. Yella, P. Gao, R. Humphry-Baker, B. F. Curchod, N. Ashari-Astani, I. Tavernelli, U. Rothlisberger, M. K. Nazeeruddin, and M. Grätzel, *Nat. Chem.* **6**, 242 (2014).
- [7] D. Sampedro, *Phys. Chem. Chem. Phys.* **13**, 5584 (2011).
- [8] R. Losantos, I. Funes-Ardoiz, J. Aguilera, E. Herrera-Ceballos, C. García-Iriepa, P. J. Campos, and D. Sampedro, *Angew. Chem.* **129**, 2676 (2017).
- [9] J. Hachmann, R. Olivares-Amaya, S. Atahan-Evrenk, C. Amador-Bedolla, R. S. Sánchez-Carrera, A. Gold-Parker, L. Vogt, A. M. Brockway, and A. Aspuru-Guzik, *J. Phys. Chem. Lett.* **2**, 2241 (2011).
- [10] E. O. Pyzer-Knapp, K. Li, and A. Aspuru-Guzik, *J. Phys. Chem. Lett.* **25**, 6495 (2015).
- [11] M. Rupp, A. Tkatchenko, K.-R. Müller, and O. A. von Lilienfeld, *Phys. Rev. Lett.* **108**, 058301 (2012).
- [12] R. Ramakrishnan and O. A. von Lilienfeld, *Rev. Comput. Chem.* **30**, 225 (2017).
- [13] O. A. von Lilienfeld, *Angew. Chem. Int. Ed.* **57**, 4164 (2018).
- [14] R. Ramakrishnan and O. A. von Lilienfeld, *CHIMIA* **69**, 182 (2015).
- [15] R. Ramakrishnan, P. O. Dral, M. Rupp, and O. A. von Lilienfeld, *J. Chem. Theory Comput.* **11**, 2087 (2015).
- [16] M. Rupp, R. Ramakrishnan, and O. A. von Lilienfeld, *J. Phys. Chem. Lett.* **6**, 3309 (2015).
- [17] W. Gerrard, L. A. Bratholm, M. J. Packer, A. J. Mulholland, D. R. Glowacki, and C. P. Butts, *Chem. Sci.* **11**, 508 (2020).
- [18] A. Gupta, S. Chakraborty, and R. Ramakrishnan, *Mach. Learn.: Sci. Technol* **2**, 035010 (2021).
- [19] K. Hansen, F. Biegler, R. Ramakrishnan, W. Pronobis, O. A. von Lilienfeld, K.-R. Müller, and A. Tkatchenko, *J. Phys. Chem. Lett.* **6**, 2326 (2015).
- [20] F. A. Faber, A. S. Christensen, B. Huang, and O. A. von Lilienfeld, *J. Chem. Phys.* **148**, 241717 (2018).

- [21] Z. Qiao, M. Welborn, A. Anandkumar, F. R. Manby, and T. F. Miller III, *J. Chem. Phys.* **153**, 124111 (2020).
- [22] O. T. Unke and M. Meuwly, *J. Chem. Theory Comput.* **15**, 3678 (2019).
- [23] K. T. Schütt, P.-J. Kindermans, H. E. Sauceda, S. Chmiela, A. Tkatchenko, and K.-R. Müller, arXiv preprint arXiv:1706.08566 (2017).
- [24] F. A. Faber, L. Hutchison, B. Huang, J. Gilmer, S. S. Schoenholz, G. E. Dahl, O. Vinyals, S. Kearnes, P. F. Riley, and O. A. von Lilienfeld, *J. Chem. Theory Comput.* **13**, 5255 (2017).
- [25] P. Hohenberg and W. Kohn, *Phys. Rev.* **136**, B864 (1964).
- [26] E. Runge and E. K. Gross, *Phys. Rev. Lett.* **52**, 997 (1984).
- [27] C. D. Rankine and T. J. Penfold, *J. Phys. Chem. A* **125**, 4276 (2021).
- [28] R. Ramakrishnan, M. Hartmann, E. Tapavicza, and O. A. von Lilienfeld, *J. Chem. Phys.* **143**, 084111 (2015).
- [29] E. Tapavicza, G. F. von Rudorff, D. O. De Haan, M. Contin, C. George, M. Riva, and O. A. von Lilienfeld, *Environ. Sci. Technol.* **55**, 8447– (2021).
- [30] Z. Liu, L. Lin, Q. Jia, Z. Cheng, Y. Jiang, Y. Guo, and J. Ma, *J. Chem. Inf. Model.* **61**, 1066 (2021).
- [31] B. Mazouin, A. A. Schöpfer, and O. A. von Lilienfeld, arXiv preprint arXiv:2110.02596 (2021).
- [32] O. Çaylak and B. Baumeier, *J. Chem. Theory Comput.* **17**, 4891 (2021).
- [33] J. Westermayr and P. Marquetand, *J. Chem. Phys.* **153**, 154112 (2020).
- [34] J. Westermayr and P. Marquetand, *Chem. Rev.* **121**, 9873–9926 (2020).
- [35] P. O. Dral and M. Barbatti, *Nat. Rev. Chem.* **5**, 388 (2021).
- [36] K. Hansen, G. Montavon, F. Biegler, S. Fazli, M. Rupp, M. Scheffler, O. A. von Lilienfeld, A. Tkatchenko, and K.-R. Müller, *J. Chem. Theory Comput.* **9**, 3404 (2013).
- [37] O. A. von Lilienfeld, R. Ramakrishnan, M. Rupp, and A. Knoll, *Int. J. Quantum Chem.* **115**, 1084 (2015).
- [38] X. Huang, B. J. Braams, and J. M. Bowman, *J. Chem. Phys.* **122**, 044308 (2005).
- [39] J. Behler, *Int. J. Quantum Chem.* **115**, 1032 (2015).
- [40] S. Manzhos and T. Carrington Jr, *Chem. Rev.* **121**, 10187–10217 (2020).
- [41] C. B. Mahmoud, A. Anelli, G. Csányi, and M. Ceriotti, *Phys. Rev. B* **102**, 235130 (2020).
- [42] J. Westermayr and R. J. Maurer, *Chem. Sci.* **12**, 10755–10764 (2021).
- [43] T. Korona and H.-J. Werner, *J. Chem. Phys.* **118**, 3006 (2003).
- [44] C. Adamo and V. Barone, *J. Chem. Phys.* **110**, 6158 (1999).
- [45] A. D. Laurent and D. Jacquemin, *Int. J. Quantum Chem.* **113**, 2019 (2013).
- [46] D. Jacquemin, E. A. Perpète, G. E. Scuseria, I. Ciofini, and C. Adamo, *J. Chem. Theory Comput.* **4**, 123 (2008).
- [47] D. Jacquemin, V. Wathelet, E. A. Perpète, and C. Adamo, *J. Chem. Theory Comput.* **5**, 2420 (2009).
- [48] P.-F. Loos, A. Scemama, A. Blondel, Y. Garniron, M. Caffarel, and D. Jacquemin, *J. Chem. Theory Comput.* **14**, 4360 (2018).
- [49] P.-F. Loos, F. Lipparini, M. Boggio-Pasqua, A. Scemama, and D. Jacquemin, *J. Chem. Theory Comput.* **16**, 1711 (2020).
- [50] A. Chrayteh, A. Blondel, P.-F. Loos, and D. Jacquemin, *J. Chem. Theory Comput.* **17**, 416 (2020).
- [51] P.-F. Loos, A. Scemama, M. Boggio-Pasqua, and D. Jacquemin, *J. Chem. Theory Comput.* **16**, 3720 (2020).
- [52] R. Send, M. Kühn, and F. Furche, *J. Chem. Theory Comput.* **7**, 2376 (2011).
- [53] R. Berraud-Pache, F. Neese, G. Bistoni, and R. Izsák, *J. Chem. Theory Comput.* **16**, 564 (2020).
- [54] C. W. Murray, S. C. Racine, and E. R. Davidson, *J. Comput. Phys.* **103**, 382 (1992).
- [55] M. E. Casida, C. Jamorski, K. C. Casida, and D. R. Salahub, *J. Chem. Phys.* **108**, 4439 (1998).
- [56] M. E. Casida and M. Huix-Rotllant, *Annu. Rev. Phys. Chem.* **63**, 287 (2012).
- [57] L. A. Curtiss, P. C. Redfern, and K. Raghavachari, *Wiley Interdiscip. Rev. Comput. Mol. Sci.* **1**, 810 (2011).
- [58] L. A. Curtiss, P. C. Redfern, and K. Raghavachari, *J. Chem. Phys.* **123**, 124107 (2005).
- [59] S. K. Das, S. Chakraborty, and R. Ramakrishnan, *J. Chem. Phys.* **154**, 044113 (2021).
- [60] J.-D. Chai and M. Head-Gordon, *Phys. Chem. Chem. Phys.* **10**, 6615 (2008).
- [61] S. Senthil, S. Chakraborty, and R. Ramakrishnan, *Chem. Sci.* **12**, 5566 (2021).
- [62] T. Fink, H. Bruggesser, and J.-L. Reymond, *Angew. Chem. Int. Ed.* **44**, 1504 (2005).
- [63] T. Fink and J.-L. Reymond, *J. Chem. Inf. Model.* **47**, 342 (2007).
- [64] L. C. Blum and J.-L. Reymond, *J. Am. Chem. Soc.* **131**, 8732 (2009).
- [65] L. Ruddigkeit, R. Van Deursen, L. C. Blum, and J.-L. Reymond, *J. Chem. Inf. Model.* **52**, 2864 (2012).
- [66] G. Montavon, M. Rupp, V. Gobre, A. Vazquez-Mayagoitia, K. Hansen, A. Tkatchenko, K.-R. Müller, and O. A. von Lilienfeld, *New J. Phys.* **15**, 095003 (2013).
- [67] J. Hoja, L. M. Sandonas, B. G. Ernst, A. Vazquez-Mayagoitia, R. A. DiStasio Jr, and A. Tkatchenko, *Sci. Data* **8**, 1 (2021).
- [68] R. Ramakrishnan, P. O. Dral, M. Rupp, and O. A. von Lilienfeld, *Sci. Data* **1**, 1 (2014).
- [69] P. Kayastha and R. Ramakrishnan, “bigQM7 ω : A high-quality dataset of ground-state properties and excited state spectra of 12880 molecules containing up to 7 atoms of CONF,” (2021).
- [70] J. P. Perdew, K. Burke, and M. Ernzerhof, *Phys. Rev. Lett.* **77**, 3865 (1996).
- [71] A. D. Becke, *J. Chem. Phys.* **98**, 1372 (1993).
- [72] P. Kayastha and R. Ramakrishnan, “bigQM7 ω : Unstructured data on NOMAD repository,” (2021).
- [73] A. K. Rappé, C. J. Casewit, K. Colwell, W. A. Goddard III, and W. M. Skiff, *J. Am. Chem. Soc.* **114**, 10024 (1992).
- [74] N. M. O’Boyle, M. Banck, C. A. James, C. Morley, T. Vandermeersch, and G. R. Hutchison, *J. Cheminformatics* **3**, 1 (2011).
- [75] M. Frisch, G. Trucks, H. Schlegel, G. Scuseria, M. Robb, J. Cheeseman, G. Scalmani, V. Barone, G. Petersson, H. Nakatsuji, *et al.*, “Gaussian 16,” (2016).
- [76] B. Schölkopf, A. J. Smola, F. Bach, *et al.*, *Learning with kt vector machines, regularization, optimization, and beyond* (MIT press, 2002).

- [77] A. S. Christensen, L. A. Bratholm, F. A. Faber, and O. Anatole von Lilienfeld, *J. Chem. Phys.* **152**, 044107 (2020).
- [78] B. Huang and O. A. von Lilienfeld, *Nat. Chem.* **12**, 945 (2020).
- [79] P. Kayastha and R. Ramakrishnan, *Mach. Learn.: Sci. Technol* **2**, 035035 (2021).
- [80] C. F. Van Loan and G. Golub, *Matrix computations (Johns Hopkins studies in mathematical sciences)* (The Johns Hopkins University Press, 1996).
- [81] A. Christensen, F. Faber, B. Huang, L. Bratholm, A. Tkatchenko, K. Muller, and O. von Lilienfeld, "QML: A python toolkit for quantum machine learning," (2017).
- [82] A. Gupta, S. Chakraborty, D. Ghosh, and R. Ramakrishnan, arXiv preprint arXiv:2110.05414 (2021).
- [83] L. Igual and S. Seguí, *Introduction to Data Science* (Springer, 2017) pp. 1–4.
- [84] N. J. Turro, V. Ramamurthy, and J. C. Scaiano, *Modern molecular photochemistry of organic molecules* (Viva Books University Science Books, Sausalito, 2017).
- [85] S. H. Vosko, L. Wilk, and M. Nusair, *Can. J. Phys.* **58**, 1200 (1980).
- [86] J. P. Perdew, P. Ziesche, and H. Eschrig, *Electronic structure of solids* (Akademie Verlag, Berlin, 1991).
- [87] C. Lee, W. Yang, and R. G. Parr, *Phys. Rev. B* **37**, 785 (1988).
- [88] J. Tao, J. P. Perdew, V. N. Staroverov, and G. E. Scuseria, *Phys. Rev. Lett.* **91**, 146401 (2003).
- [89] Y. Zhao and D. G. Truhlar, *Theor. Chem. Acc.* **120**, 215 (2008).
- [90] R. Peverati and D. G. Truhlar, *J. Phys. Chem. Lett.* **2**, 2810 (2011).
- [91] H. Iikura, T. Tsuneda, T. Yanai, and K. Hirao, *J. Chem. Phys.* **115**, 3540 (2001).
- [92] O. A. Vydrov and G. E. Scuseria, *J. Chem. Phys.* **125**, 234109 (2006).
- [93] T. Yanai, D. P. Tew, and N. C. Handy, *Chem. Phys. Lett.* **393**, 51 (2004).
- [94] J. P. Perdew and K. Schmidt, *AIP Conf. Proc.*, **577**, 1 (2001).
- [95] L. Zheng, N. F. Polizzi, A. R. Dave, A. Migliore, and D. N. Beratan, *J. Phys. Chem. A* **120**, 1933 (2016).
- [96] F. Plasser, *J. Chem. Phys.* **152**, 084108 (2020).
- [97] A. H. Motagamwala and J. A. Dumesic, *Chem. Rev.* **121**, 1049 (2020).
- [98] W. Boehm and H. Prautzsch, *Numerical Methods* (AK Peters Ltd., Wellesley, MA, 1993).